Applied Catalysis B: Environmental 166–167 (2015) 25–31

Contents lists available at ScienceDirect

Applied Catalysis B: Environmental

journal homepage: www.elsevier.com/locate/apcatb

Selective electro-oxidation of glycerol over Au supported on extended poly(4-vinylpyridine) functionalized graphene

Haibo Wang[a], Larissa Thia[b], Nan Li[a], Xiaoming Ge[c], Zhaolin Liu[c], Xin Wang[a,*]

[a] School of Chemical and Biomedical Engineering, Nanyang Technological University, 62 Nanyang Drive, Singapore 637459, Singapore
[b] Interdisciplinary Graduate School, Nanyang Technological University, 50 Nanyang Avenue, Block S2-B3a-01, Singapore 639798, Singapore
[c] Institute of Materials Research and Engineering, Agency for Science, Technology and Research (A*STAR), 3 Research Link, Singapore 117602, Singapore

ARTICLE INFO

Article history:
Received 5 May 2014
Received in revised form 21 August 2014
Accepted 3 November 2014
Available online 13 November 2014

Keywords:
Glycerol oxidation
Selectivity
d-Band center
Gold nanoparticle
Graphene

ABSTRACT

Au nanoparticles (NPs) supported on various supports with different metal support interaction are synthesized and tested for glycerol electro-oxidation. Through off-line HPLC analysis, it is found that Au NPs supported on extended poly(4-vinylpyridine) functionalized graphene (Au-P4P/G) shows a much higher activity and much better selectivity for three carbon products than those on carbon black, P4P functionalized reduced graphene oxide (Au-P4P/rGO) and poly(*m*-aminophenol) (PmAP) wrapped graphene (Au-PmAP/G), e.g., the glyceric acid production reaches 68.6% at 0.2 V (vs. HgO/Hg), and the ratio between three carbon products and other products is 4.92 for Au-P4P/G compared with 0.96 of Au-CB. XPS results indicate that lower d-band center in Au nanoparticles induces higher three carbon selectivity and the changed adsorption ability for oxygen-containing groups might be the main reason.

1. Introduction

Glycerol is a potential fuel for fuel cells due to its non-toxicity and low volatility [1,2]. Recently the boom of biodiesel production has produced large amount of glycerol as byproduct [3,4], this causes a drastic decline in the price of glycerol globally [5–7]. In order to increase the adding value, generating the power from fuel cell while also selectively converting glycerol into other valuable chemicals, such as glyceric acid, tartronic acid, dihydroxyacetone and mesoxalic acid, is highly preferred [8–11].

Selective electro-oxidation can be achieved through the mediation of other molecules or cations. An earlier work revealed that glycerol could be selectively electro-oxidized to 1,3-dihydroxyacetone (DHA) in the presence of TEMPO (2,2,6,6-tetramethylpiperidine-1-oxyl) [12]. Recently Kwon et al. showed that glycerol was fully converted to DHA at carbon support Pt electrode in bismuth saturated solution [9]. It was suggested the interaction between Bi and the primary hydroxy groups played an important role. Other works focused on different catalysts and working conditions to control the electro-oxidation process. Li et al. applied carbon supported Pt and Au catalysts in an anion-exchange membrane fuel cell (AEMFC). High selectivity towards tartronic acid, glycolic acid, mesoxalic acid would be obtained through careful control of working conditions [10,13,14]. Pd based catalysts have also been studied [8,11]. It is noteworthy that Pd-(Ni—Zn) on carbon produced both a higher current density and improved selectivity in AEMFC [11].

On the other hand, Au NPs have been widely studied because of its enhanced selectivity in the liquid phase oxidation [15–17]. Selectivity of glyceric acid can reach 100% under optimized conditions [15]. However, in the electro-oxidation, the glyceric acid production only dominated at potential lower than the onset potential (0.8 V vs. RHE) in the three electrode cell. At potential higher than the onset potential, two-carbon (glycolic acid) and one-carbon (formic acid) products are predominant in the largest proportions (~90%) [18]. This is also confirmed in this paper by using Au NPs on carbon black.

Here, we choose Au supported on extended poly(4-vinylpyridine) wrapped graphene as the catalyst to selectively oxidize glycerol into glyceric acid during electro-oxidation of glycerol. Although several ways including introducing foreign substances and controlling working potential have been developed to selectively electro-oxidize glycerol, there have been few studies conducted to determine the impact of the intrinsic electronic properties of catalyst via metal-support interaction during the electro-oxidation process. Most studies focus on the influence of electronic structure of metal catalysts for their oxidation activity [19–21]. Through carefully controlling the interaction between Au NPs and polymer on graphene surface, we obtained Au based catalysts with varying extents of electron enrichment. Different

* Corresponding author. Tel.: +65 6316 8866; fax: +65 6794 7553.
E-mail address: WangXin@ntu.edu.sg (X. Wang).

http://dx.doi.org/10.1016/j.apcatb.2014.11.009
0926-3373/

with conventional designed polymer wrapped carbon material, the highly extended polymer wrapped graphene in this paper shows a more powerful ability to alter the intrinsic electronic property of Au NPs, which resulted in a higher selectivity toward three-carbon products with good activity.

2. Experimental

2.1. Materials

Poly(4-vinylpyridine) (P4P, *MW* = 160,000) were purchased from Sigma-Aldrich. Poly(*m*-aminophenol) (PmAP) was prepared according to previous literature procedure [22].

2.2. Preparation of catalysts

For polymer functionalized graphene (polymer/G) [23], 0.04 g polymer was dissolved into 0.8 ml DMSO, followed by the addition of 0.1 g graphite. After ultrasonication for 20 h, the black solution was placed overnight and the sediment was discarded. Then polymer wrapped graphene in the upper solution was washed by centrifuging at 10,000 rpm for several times. Specifically, PmAP wrapped graphene was washed with 0.01 M NaOH, P4P/graphene was washed with 0.02 M HCl. Finally the synthesized polymer/graphene was dispersed in aqueous solution.

For P4P functionalized reduced graphene oxide (P4P/rGO), rGO was synthesized according to the literature [24]. Briefly, 12.5 mg GO was dissolved into 50 ml DI water, then 13.5 μl $N_2H_4{\cdot}H_2O$ (64–65%) solution was added, followed by 0.175 ml 25% NH_4OH. The product was collected and centrifuged after slowly stirring at 90 °C for 90 min. After that, the synthesized rGO was dissolved into 40 ml 1:1 (v/v) ethanol/water mixed solvent. Meanwhile, 0.125 g P4P was dissolved into 60 ml 1:1 (v/v) ethanol/water mixed solvent. After mixing and stirring overnight, polymer wrapped rGO was purified by centrifuging three times with ethanol. Finally it was stored in ethanol solution.

To prepare Au loaded carbon black (Au-CB), P4P/graphene (Au-P4P/G), PmAP/graphene (Au-PmAP/G) and P4P/rGO (Au-P4P/rGO), first Au nanoparticles are synthesized as follows: 4 nm Au solution was prepared by adding 1 ml 1% $HAuCl_4{\cdot}3H_2O$ to 100 ml DI water, after stirring 1 min, 1 ml 1% aqueous sodium citrate solution was added. 1 min later, 1 ml fresh prepared 0.075% $NaBH_4$ in 1% sodium citrate was quickly added. The solution was continuously stirred for 5 min and then stored at 4 °C. Then appropriate amount of support dispersion and Au nanoparticle solution were mixed under ultrasonication for 1 h. The mixture was stirred overnight, with the pH adjusted below 2 by using 0.2 M HCl. Continuously stirring for 1 h, the product was centrifuged at 10,000 rpm and washed with DI water three times. Then the product was dried below 80 °C.

2.3. Physicochemical characterization

The morphology was observed by using transmission electron microscopy (TEM) at JEOL JEM-3010. The X-ray diffraction patterns are collected by Bruker D2 Phaser. Thermo gravimetric analysis (TGA) was carried out at SDT Q600 with a temperature ramp rate of 10 °C under air atmosphere. The atomic force microscope (AFM) images of various samples on mica were collected at MFP-3D-SA (Asylum Research) in AC mode. The X-ray photoelectron spectroscopy (XPS) spectra were collected at VG ESCALAB 200i-XL after coating samples with Pt. Pt(0) $4f_{7/2}$ and $4f_{5/2}$ at 71.1 and 74.4 eV were used as the reference for charge correction [25].

2.4. Electrochemical characterization

All electrochemical tests were carried out at room temperature in conventional three-electrode cell using Autolab PGSTAT302 potentiostat. Pt foil and Hg/HgO (6 M KOH) were used as the counter and reference electrode, glassy carbon electrode with 5 mm diameter and carbon cloth (1.4 × 1.4 cm^2, Gashub) were used as the working electrode. The sample was prepared following the below procedure: firstly 2 mg catalyst was dispersed in 2.5 ml ethanol solution by ultrasonication for 5 min; then 0.5 ml 0.05 wt% Nafion solution was added, ultrasonicating for 10 min to obtain the black dispersion. In the cyclic voltammograms (CV) test, 30 μl catalyst dispersion was dropped on the glassy carbon electrode. After drying, the test was conducted in the 0.5 M NaOH + 0.5 M glycerol solution. The electrochemical impedance spectroscopy (EIS) test was operated at open-circuit potential, Ag/AgCl (saturated KCl) was used as reference electrode. The supporting solution was prepared by using 5 mM $K_3[FeCN_6]/K_4[FeCN_6]$ (1:1) as redox probe and 0.1 M KCl as supporting electrolyte. In the chronoamperometric experiments, 0.02 mg catalyst was dropped onto glassy carbon (GC) and 0.2 mg, 1 mg and 2 mg catalyst was dropped onto carbon cloth (CC). The working electrode was firstly immersed in 0.5 M NaOH + 0.5 M glycerol under stirring for 10 h to fully saturate the electrode, then washed carefully with DI water. After that, it was immersed inside 20 ml 0.5 M NaOH + 0.5 M glycerol solution during the test. After setting and applying the specific potential on the working electrode for 2 h, 1 ml solution was collected for the high performance liquid chromatography (HPLC) analysis.

2.5. Chromatographic determination of products

The obtained products were analyzed by high performance liquid chromatography (HPLC, Agilent 1260 Infinity). The determination of oxalic acid was conducted by Alltech OA-1000 Organic Acid column. In other cases, column Aminex HPX 87-H (Bio-Rad) was used. The eluent was sulfuric acid (4 mM). During the test, 20 μL sample was injected into the column and the temperature of the column was kept at 65 °C. The flow rate was 0.2 ml/min. The separated compounds were detected with both the refractive index (RID) detector and UV–vis detector. The expected glycerol oxidation products were analyzed at the same condition to produce the calibration curves (glyceric acid, glycolic acid, formic acid, oxalic acid, and tartronic acid).

3. Results and discussions

Four different materials, including carbon black (CB), Poly(*m*-aminophenol) and Poly(4-vinylpyridine) wrapped graphene (PmAP/G and P4P/G), Poly(4-vinylpyridine) functionalized reduced graphene oxide (P4P/rGO), were carefully chosen as support in this work. CB has weak interaction with Au NPs because few functional groups on the surface. PmAP and P4P functionalized graphene can donate a pair of electrons generated from —N= groups although in PmAP most —N= groups form the hydrogen bond with —OH groups [22], inducing a different extent of electron donation from support to Au NPs. The use of P4P/rGO is to examine the effect of support conductivity. PmAP/G and P4P/G were synthesized through ultrasonication and P4P/rGO was obtained by chemical reduction. Then as-synthesized Au nanoparticles were loaded onto these supports and also CB. The morphology of Au nanoparticles was investigated by TEM and XRD. TEM images show that Au NPs are homogeneously deposited onto different support surface (Fig. 1a–d). As catalysts are prepared from the same sol–gel solution, Au NPs exhibit similar particle size distribution in all

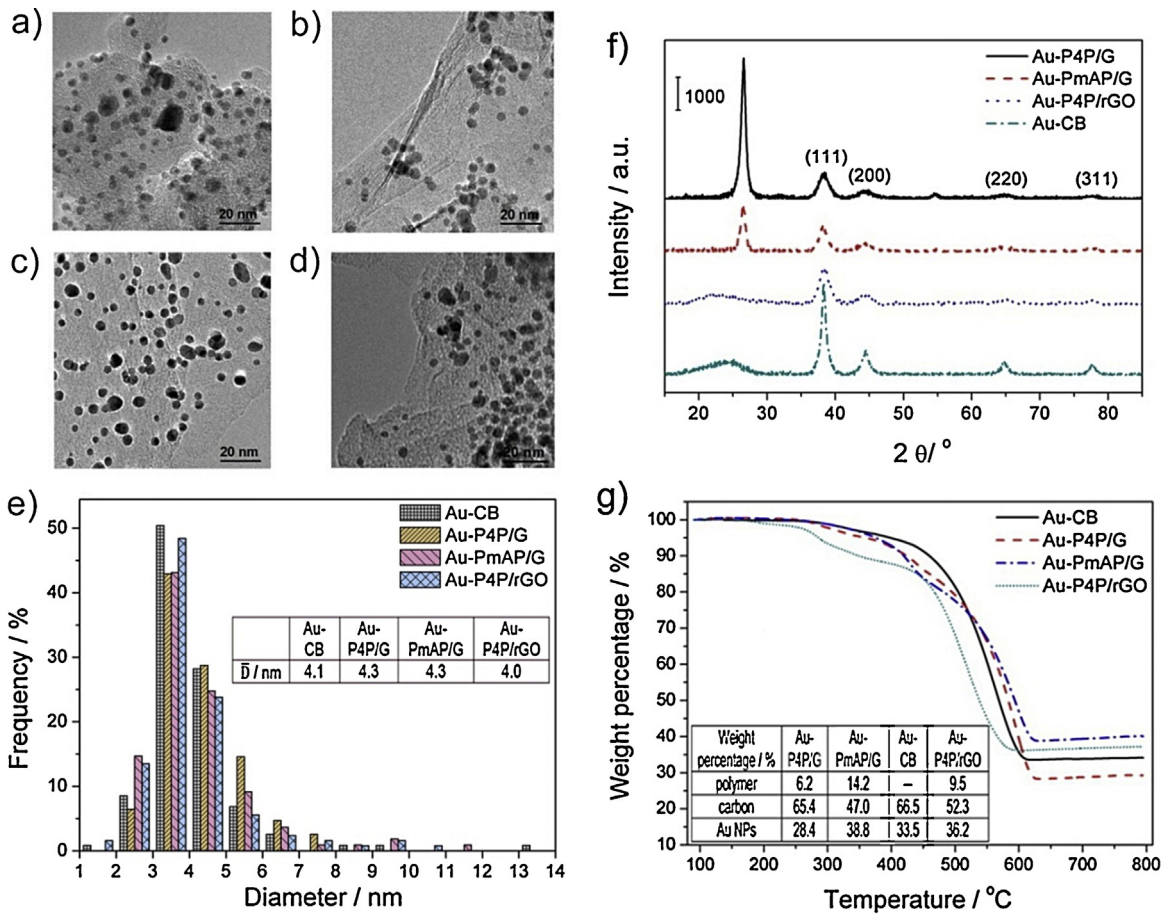

Fig. 1. TEM images of (a) Au-CB, (b) Au-P4P/G, (c) Au-PmAP/G, and (d) Au-P4P/rGO. (e) The particle size histogram of Au-CB, Au-P4P/G, Au-PmAP/G, and Au-P4P/rGO. (f) X-ray diffraction (XRD) patterns of Au-P4P/G, Au-PmAP/G, Au-P4P/rGO and Au-CB. (g) Thermal gravimetric analysis (TGA) of Au-P4P/G, Au-PmAP/G, Au-CB and Au-P4P/rGO in air atmosphere.

these catalysts (Fig. 1e). The calculated average diameter of Au NPs in Au/CB, Au-P4P/G, Au-PmAP/G and Au-P4P/rGO is 4.1, 4.3, 4.3 and 4.0 nm, respectively. XRD was also conducted to characterize catalysts (Fig. 1f). Peaks in the range from 22° to 26° are ascribed to the inter-spacing of (0 0 2) graphite planes. Peaks appearing at 38.2°, 44.5°, 64.7° and 77.8° are assigned to the (1 1 1), (2 0 0), (2 2 0) and (3 1 1) planes of face-centered-cubic (FCC) Au. Based on the Debye–Scherrer equation, the calculated average size of Au NPs on P4P/G, PmAP/G and P4P/rGO is 4.8, 4.9 and 4.6 nm while that on CB is 7.9 nm. The particle size of Au NPs on CB calculated via XRD is much larger than that from TEM. This may be caused by the aggregation of Au nanoparticles on carbon black due to the relatively weak interaction between CB and Au. The weight percentage of different components in catalysts was analyzed by TGA (Fig. 1g). For Au-CB, weight loss at low temperature (<400 °C) may be induced from the decomposition of amorphous carbon [26]. While for other samples, the weight loss from 220 to 400 °C is largely caused by the decomposition of polymer and below 220 °C is ascribed to absorbed water or residual functional groups on rGO [27,28]. Oxidation of carbon occurs at higher temperatures (400–600 °C). Final Au loading on P4P/G, PmAP/G, CB and P4P/rGO is 28%, 39%, 34% and 36%, respectively.

The products of glycerol electro-oxidation were determined by HPLC (Fig. S1). Oxalic acid, tartronic acid, glyceric acid and glycolic acid were detected by RID detector and formic acid was analyzed by UV–vis detector. Production of mesoxalic acid has been reported when glycerol oxidation was carried out on Pt and Au based catalysts [10,13]. However, in our study only oxalic acid was observed. This was ascertained by comparing the retention time of mesoxalic acid and oxalic acid standards (Fig. S2).

We then compared the electrocatalytic activity of Au NPs loaded on different supports. In the CV test, with the increase of potential, the glycerol oxidation peak appears at around 0.5 V (vs. HgO/Hg) for Au-CB, Au-P4P/G and Au-PmAP/G. During the reverse scan, another oxidation peak appears at around 0.2 V (vs. HgO/Hg) for Au-CB, Au-P4P/G and Au-PmAP/G, which is again ascribed to the glycerol oxidation after the reactivation of catalyst surface. Among these three catalysts, Au-CB and Au-PmAP/G exhibit similar oxidation current density which are much lower than that of Au-P4P/G (Fig. 2a). This also corresponds to the activity normalized by the electrochemical active surface area (Fig. S3). It indicates that Au-P4P/G possesses higher electrocatalytic activity. Moreover, Au-P4P/rGO shows no obvious glycerol oxidation peak. This means the oxidation of glycerol is very sluggish over Au-P4P/rGO. EIS test was conducted to extract the equivalent series resistance ESR and charge transfer resistance R_{ct} (Fig. 2b) [29]. ESR which includes resistances from electrolytes, electrodes and electrical contacts is used to compare the conductivity of catalysts, as the remaining parts in the three electrode cell are the same. ESR of Au-CB, Au-PmAP/G, Au-P4P/G and Au-P4P/rGO is around 68, 73, 72 and 76 Ω and R_{ct} is 22.2, 83.1, 245.7, 613.9 Ω, respectively. The low conductivity and high R_{ct} of Au-P4P/rGO induces its low activity. For the case of Au-P4P/G, although its conductivity is lower and charge transfer resistance is higher than Au-CB, higher activity was observed, indicating some other factors also play important role in the electrocatalytic activity, other than the conductivity. A possible

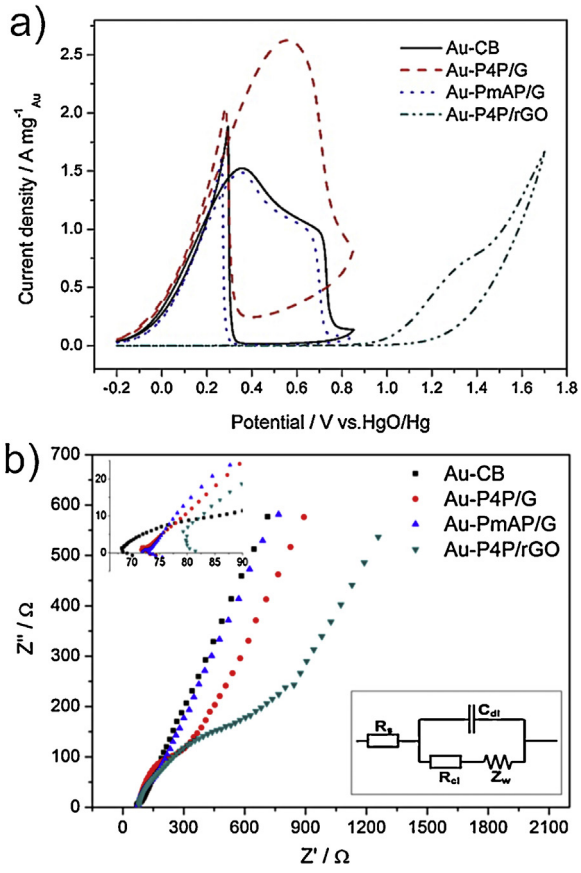

Fig. 2. Cyclic voltammograms (CV) of Au-CB, Au-P4P/G, Au-PmAP/G and Au-P4P/rGO in 0.5 M glycerol + 0.5 M NaOH with a scan rate of 50 mV/s. (b) Nyquist impedance plots of Au-CB, Au-P4P/G, Au-PmAP/G and Au-P4P/rGO. Frequency range: 0.01—10,000 Hz. Inset are the equivalent circuit and the enlarged spectra of catalysts at high frequency region.

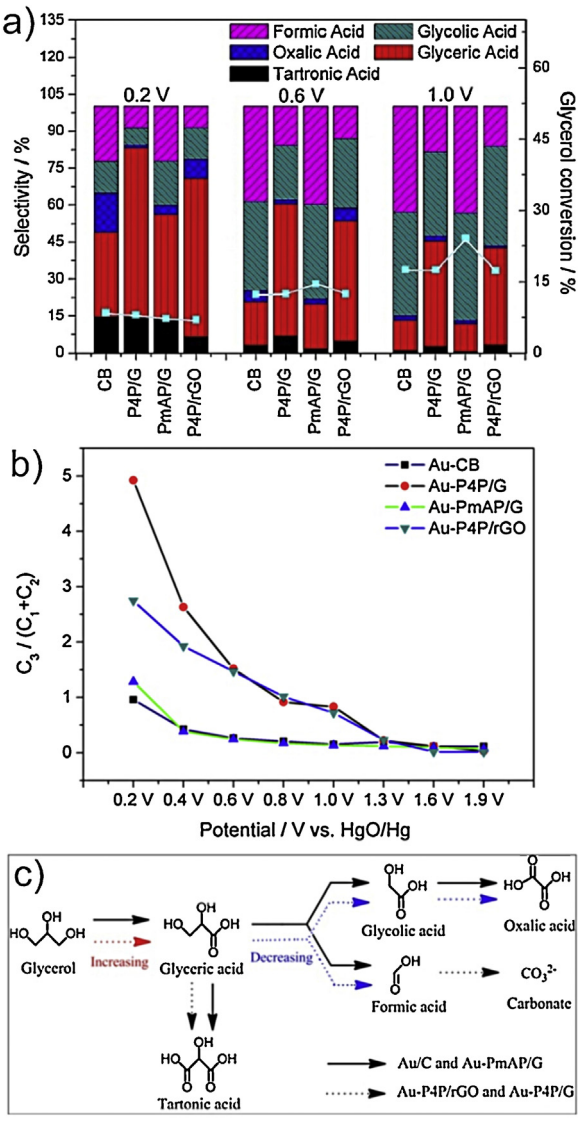

Fig. 3. (a) The product selectivity and glycerol conversion (b) The three-carbon products selectivity over Au on different supports (CB, P4P/G, PmAP/G and P4P/rGO) at various potentials. The catalyst loading is 1 mg cm^{-2} and the working electrode is carbon cloth. Reproducibility test shows the deviation is within 10%. (c) The scheme of glycerol oxidation over Au/C, Au-PmAP/G, Au-P4P/rGO and Au-P4P/G. Red color arrow means the reaction yield is increased while the blue arrow means the yield is decreased. (For interpretation of the references to color in this figure legend, the reader is referred to the web version of this article.)

reason might be the appropriate adsorption strength of the species on the catalysts surface via the tuning of the d-band center [19–21]. Details will be discussed in the later session.

The activity of different catalysts was also investigated by HPLC after holding at a series of potentials in 0.5 M NaOH + 0.5 M glycerol solution for 2 h, these potentials are much higher than the onset potential (around −0.2 V vs. HgO/Hg). It should be mentioned that only supports without Au NPs show no activity (Fig. S4). During the test, it was observed that higher potential commonly leads to higher glycerol conversion (Fig. 3a). Among these catalysts, Au-P4P/G shows higher activity than Au-CB and Au-P4P/rGO as observed from their similar glycerol conversion despite its lower Au loading (Fig. 1g). This agrees with the results from CV test (Fig. 2a). Apart from the activity, Au NPs on different supports also show very diverse selectivity for glycerol oxidation. Au NPs on either CB or PmAP/G have very similar selectivity. After changing polymer from PmAP to P4P on exfoliated graphene surface, the production of glyceric acid is largely enhanced, e.g., when the potential is 0.2 V, the glyceric acid production in Au-CB, Au-PmAP, Au-P4P/rGO and Au-P4P/G are 34.5%, 42.2%, 57.4% and 68.6% while the glycolic acid production are 12.7%, 17.8%, 11.3% and 7.0%, respectively (Fig. 3a). The selectivity of 3-carbon products especially glyceric acid is much higher for Au-P4P/rGO and Au-P4P/G than Au-CB and Au-PmAP/G throughout the low to medium potential range (0.2–1 V, Fig. 3b). Since glyceric acid is easily to be oxidized into glycolic acid and formic acid on Au at high potential [18], the enhanced production of glyceric acid means that further oxidation on Au-P4P/rGO and Au-P4P/G is effectively hindered (Fig. 3c). Interestingly, the production of formic acid is roughly equal to the production of glycolic acid and oxalic acid for Au-CB and Au-PmAP/G between 0.2 V to 1 V, while for Au-P4P/rGO and Au-P4P/G, the production of formic acid is less than the production of two carbon products. This indicates that the formic acid in Au-P4P/rGO and Au-P4P/G is more easily oxidized into carbonate (Fig. 3c) [18]. Even after taking the production of carbonate into account (Fig. S5), we can still reach the same conclusion that P4P/G shows improved selectivity towards three carbon products.

To understand the different activity and selectivity of Au NPs, we studied the electronic structure of Au NPs on different supports by XPS spectra after the samples are coated and calibrated by Pt (Fig. S6). Peaks corresponding to the Au $4f_{7/2}$ core level of Au-CB, Au-PmAP/G, Au-P4P/rGO and Au-P4P/G are at 82.65, 82.55, 82.41 and 82.19 eV (Fig. 4d), respectively. Since Au NPs on different supports possess almost the same particle size, the influence of the particle size for XPS can be excluded [30]. So the shift of Au $4f_{7/2}$ peak

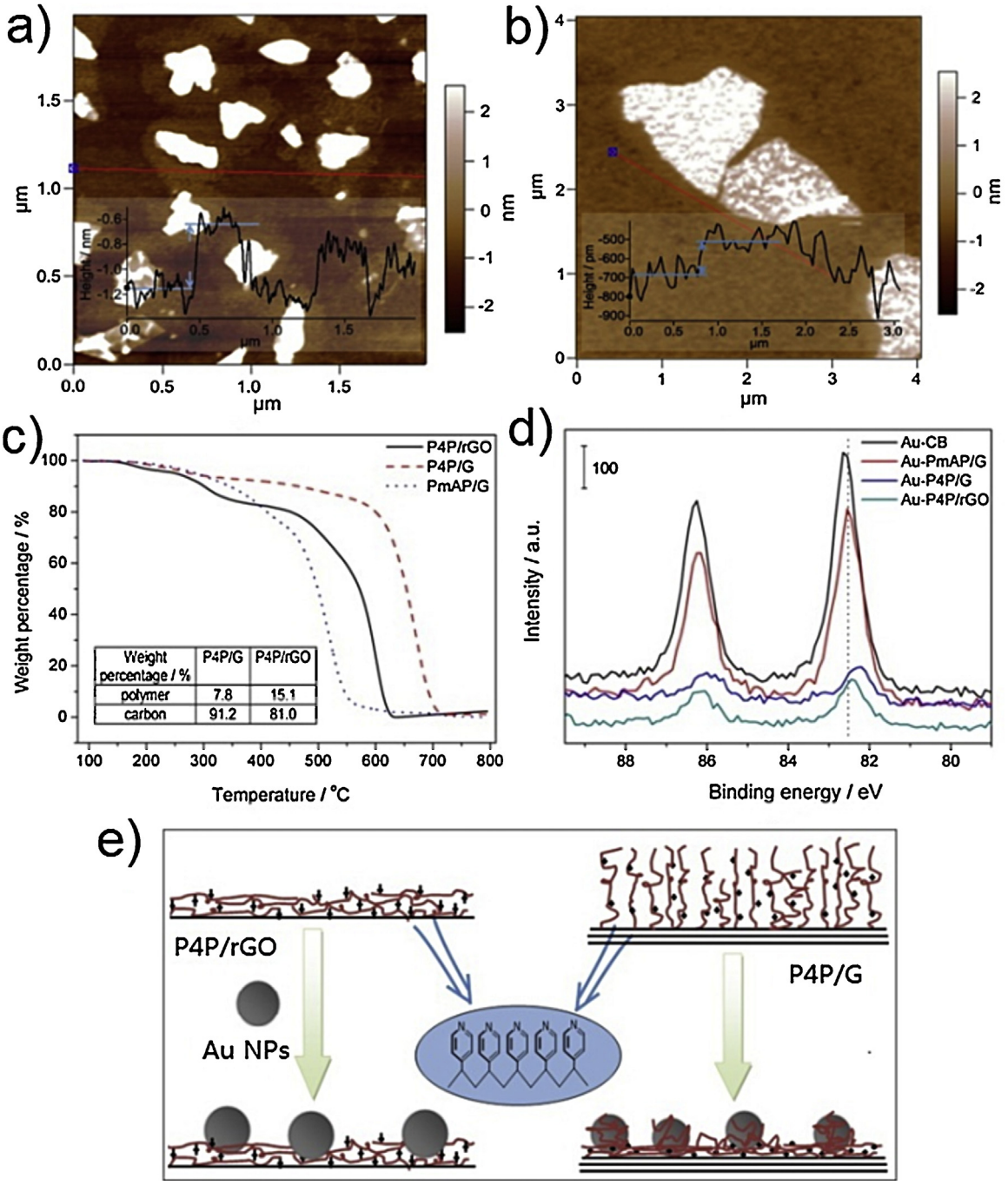

Fig. 4. AFM height images of (a) P4P/G and (b) P4P/rGO deposited on mica surface. (c) TGA curves of P4P/G, P4P/rGO and rGO in air atmosphere. (d) The XPS spectra of Au 4f in Au-CB, Au-PmAP/G, Au-P4P/G and Au-P4P/rGO. (e) The schematic drawing of the loading of Au NPs on P4P/rGO and P4P/G.

to a lower binding energy on graphene and rGO supported samples could be explained by the negatively charged Au NPs [19,21], which means a lower d-band center. Among these catalysts, —N= group in the PmAP chain shows much weaker electron-donating ability compared with pyridine group in P4P chain due to its hydrogen bonding with the *m*-position —OH group [22]. This leads to a slightly decrement of Au $4f_{7/2}$ peak in the Au-PmAP/G while resulting in a significant shift of Au $4f_{7/2}$ peak in P4P functionalized support. For the different electronic property between Au-P4P/rGO and Au-P4P/G, it can be ascribed to the different orientation of P4P chain on the support surface. In the AFM image of P4P/G, the thickness of polymer layer surrounding graphene is about 0.5 nm (Fig. 4a). However, the polymer thickness surrounding rGO is only about 0.1 nm when the noise of the substrate is neglected (Fig. 4b). Besides, TGA of P4P/rGO and P4P/G shows that the polymer weight percentage in P4P/G (7.8%) is much lower than that in P4P/rGO (15.1%) (Fig. 4c). Therefore, it is reasonable to conclude that above the exfoliated graphene surface most P4P chains are extended while on rGO they tend to lie on surface. This forms a much thicker polymer layer despite of the lower polymer percentage on exfoliated graphene surface, which agrees with our previous research [23]. When Au NPs are loaded, more sites of the NPs surface are wrapped by P4P, which thus induces the lowest d-band center among these four catalysts (Fig. 4e). The different extent of electron enrichment in turn induces the varied adsorption ability of oxygen containing groups for these catalysts [31]. Therefore, for Au-P4P/G, Au NPs

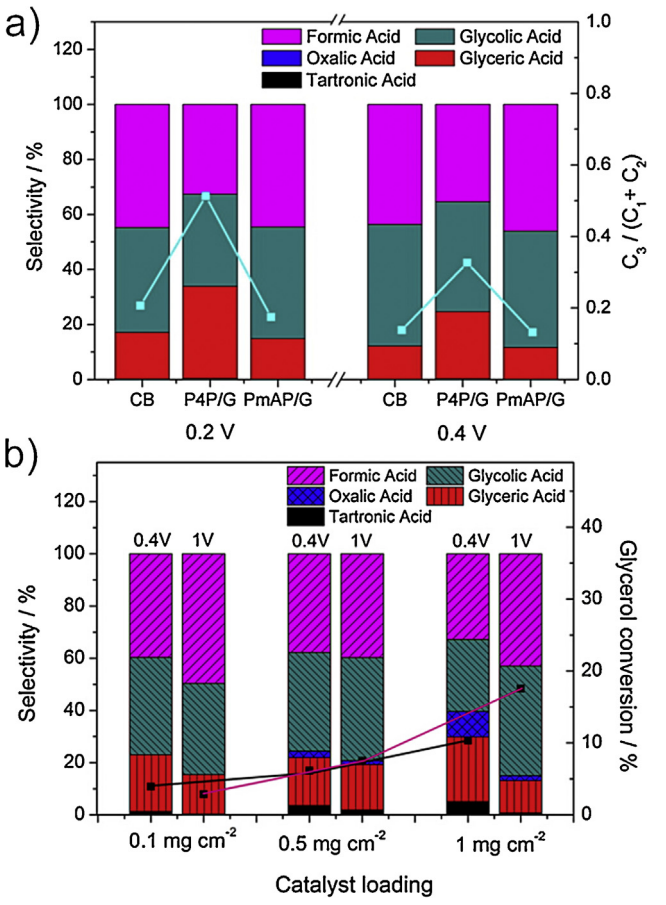

Fig. 5. (a) The product selectivity of different catalysts (Au-CB, Au-P4P/G, Au-PmAP/G) at 0.2 and 0.4 V (vs. Hg/HgO), the catalyst loading is 0.1 mg cm^{-2} and the working electrode substrate is glassy carbon. (b) The product selectivity of different loading of Au/CB at different potential (V vs. Hg/HgO) on carbon cloth electrode. The black line represents the glycerol conversion of Au/CB with varied loadings at the potential of 0.4 V, the red line represents the glycerol conversion of Au/CB with varied loadings at the potential of 1 V. (For interpretation of the references to color in this figure legend, the reader is referred to the web version of this article.)

may have the weakest adsorption ability with glyceric acid, which enhances the production of glyceric acid and hinders the further decomposition to glycolic acid and formic acid.

We also studied the effect of catalytic loading on the reaction selectivity since previous report has indicated the loading of catalysts could influence the selectivity in glycerol oxidation [10]. At the catalyst loading of 0.1 mg cm^{-2}, we observed that Au-P4P/G has better selectivity towards three-carbon products than Au-CB and Au-PmAP/G (over 2 times) (Fig. 5a). When the loading of catalyst increases, the selectivity difference is enlarged between Au-P4P/G and Au-CB (by comparing Figs. 3b and 5a). This means the increment of catalyst loading is more effective for Au-P4P/G than other catalysts in promoting the selectivity. The reason may be ascribed to the competitive adsorption between glyceric acid and other oxidized species. Since the concentration of oxidized species increases along with the catalytic loading (Fig. 5b), the adsorption competition between glyceric acid and other oxidized species would become more intense. Part of the adsorbed glyceric acid may be replaced by other oxidized species, this causes the slightly increment of the selectivity towards three carbon products in Au-CB at low potential when loading is increased. For the case of Au-P4P/G, due to its lowest d-band center, glyceric acid on the surface may be more easily replaced by other species. This caused its significant promotion in selectivity towards three carbon products when the loading is increased.

4. Conclusions

In this paper, we developed a new catalyst by loading Au NPs on extended Poly(4-vinylpyridine) (P4P) functionalized graphene for glycerol oxidation in alkaline solution. The as-synthesized Au-P4P/G shows the highest activity and selectivity towards three carbon product compared with other catalysts (Au-CB, Au-PmAP/G and Au-P4P/rGO). Due to the extended P4P chain on graphene surface in P4P/G, Au-P4P/G possesses the lowest d-band center which is confirmed by XPS analysis. On the contrary, Au NPs on carbon black and PmAP/G retain their pristine property. The lowest d-band center in Au-P4P/G causes the weakest interaction between Au NPs and glyceric acid, which makes glyceric acid easier to desorb from Au surface and hinders the further decomposition of glyceric acid into two and one carbon products. Moreover, compared to Au-P4P/rGO, Au-P4P/G obtained from the extended polymer functionalized graphene retains better conductivity which explains its much higher activity. This indicates that Au-P4P/G can serve as a potential catalyst with better control of products in the fuel cell system while producing higher current density.

Acknowledgements

We acknowledge financial support from the academic research fund AcRF tier 1 (M4011020 RG8/12) Ministry of Education, Singapore and competitive research program (2009 NRF–CRP 001–032), National Research Foundation, Singapore. The support by the Singapore National Research Foundation under its Campus for Research Excellence And Technological Enterprise (CREATE) programme is also acknowledged.

Appendix A. Supplementary data

Supplementary data associated with this article can be found, in the online version, at http://dx.doi.org/10.1016/j.apcatb.2014.11.009.

References

[1] C. Bianchini, P.K. Shen, Chem. Rev. 109 (2009) 4183–4206.
[2] E.H. Yu, U. Krewer, K. Scott, Energies 3 (2010) 1499–1528.
[3] M. McCoy, Chem. Eng. News 84 (2006) 7.
[4] E.K. Wilson, Chem. Eng. News 80 (2002) 46–49.
[5] F. Ma, M.A. Hanna, Bioresour. Technol. 70 (1999) 1–15.
[6] G.W. Huber, S. Iborra, A. Corma, Chem. Rev. 106 (2006) 4044–4098.
[7] A. Behr, J. Eilting, K. Irawadi, J. Leschinski, F. Lindner, Green Chem. 10 (2008) 13–30.
[8] M. Simões, S. Baranton, C. Coutanceau, Appl. Catal., B: Environ. 93 (2010) 354–362.
[9] Y. Kwon, Y. Birdja, I. Spanos, P. Rodriguez, M.T.M. Koper, ACS Catal. 2 (2012) 759–764.
[10] L. Xin, Z. Zhang, Z. Wang, W. Li, ChemCatChem 4 (2012) 1105–1114.
[11] A. Marchionni, M. Bevilacqua, C. Bianchini, Y. Chen, J. Filippi, P. Fornasiero, A. Lavacchi, H. Miller, L. Wang, F. Vizza, ChemSusChem 6 (2013) 518–528.
[12] R. Ciriminna, G. Palmisano, C.D. Pina, M. Rossic, M. Pagliaro, Tetrahedron Lett. 47 (2006) 6993–6995.
[13] Z. Zhang, L. Xin, W. Li, Appl. Catal., B: Environ. 119–120 (2012) 40–48.
[14] Z. Zhang, L. Xin, J. Qi, Z. Wang, W. Li, Green Chem. 14 (2012) 2150–2152.
[15] S. Carrettin, P. McMorn, P. Johnston, K. Griffin, G.J. Hutchings, Chem. Commun. (2002) 696–697.
[16] B.N. Zope, D.D. Hibbitts, M. Neurock, R.J. Davis, Science 330 (2010) 74–78.
[17] E.G. Rodrigues, S.A.C. Carabineiro, J.J. Delgado, X. Chen, M.F.R. Pereira, J.J.M. Órfão, J. Catal. 285 (2012) 83–91.
[18] Y. Kwon, K.J.P. Schouten, M.T.M. Koper, ChemCatChem 3 (2011) 1176–1185.
[19] H. Tsunoyama, N. Ichikuni, H. Sakurai, T. Tsukuda, J. Am. Chem. Soc. 131 (2009) 7086–7093.
[20] H.J. Kim, S.M. Choi, S. Green, G.A. Tompsett, S.H. Lee, G.W. Huber, W.B. Kim, Appl. Catal., B: Environ. 101 (2011) 366–375.
[21] S. Wang, F. Yang, S.P. Jiang, S. Chen, X. Wang, Electrochem. Commun. 12 (2010) 1646–1649.

[22] P. Kar, N.C. Pradhan, B. Adhikari, Mater. Chem. Phys. 111 (2008) 59–64.
[23] H. Wang, B. Xia, Y. Yan, N. Li, J.Y. Wang, X. Wang, J. Phys. Chem. B 117 (2013) 5606–5613.
[24] D. Li, M.B. Muller, S. Gilje, R.B. Kaner, G.G. Wallace, Nat. Nanotechnol. 3 (2008) 101–105.
[25] L.K. Ono, J.R. Croy, H. Heinrich, B. Roldan Cuenya, J. Phys. Chem. C 115 (2011) 16856–16866.
[26] S. Osswald, G. Yushin, V. Mochalin, S.O. Kucheyev, Y. Gogotsi, J. Am. Chem. Soc. 128 (2006) 11635–11642.
[27] R. Vijaya Kumar, Y. Koltypin, Y.S. Cohen, Y. Cohen, D. Auibach, O. Palchik, I. Felner, A. Gedanken, J. Mater. Chem. 10 (2000) 1125–1129.
[28] G. Wang, J. Yang, J. Park, X. Gou, B. Wang, H. Liu, J. Yao, J. Phys. Chem. C 112 (2008) 8192–8195.
[29] W. Sugimoto, H. Iwata, K. Yokoshima, Y. Murakami, J. Phys. Chem. B 109 (2005) 7330–7338.
[30] P. Zhang, T. Sham, Phys. Rev. Lett. 90 (2003) 245502.
[31] F.H.B. Lima, J. Zhang, M.H. Shao, K. Sasaki, M.B. Vukmirovic, E.A. Ticianelli, R.R. Adzic, J. Phys. Chem. C 111 (2007) 404–410.